ChemPubSoc Europe

DOI: 10.1002/cssc.201700864

CHEMSUSCHEM Communications

VIP *Very Important Paper*

# Metal–Organic Framework-Derived FeCo-N-Doped Hollow Porous Carbon Nanocubes for Electrocatalysis in Acidic and Alkaline Media

Xinzuo Fang[+], Long Jiao[+], Shu-Hong Yu, and Hai-Long Jiang*[a]

Metal–organic frameworks (MOFs) are ideal precursors/templates for porous carbons with homogeneous doping of active components for energy storage and conversion applications. Herein, metalloporphyrinic MOFs, PCN-224-FeCo, with adjustable molar ratio of $Fe^{II}/Co^{II}$ alternatively residing inside the porphyrin center, were employed as precursors to afford FeCo-N-doped porous carbon (denoted as FeCo-NPC) by pyrolysis. Thanks to the hollow porous structure, the synergetic effect between highly dispersed $FeN_x$ and $CoN_x$ active sites accompanied with a high degree of graphitization, the optimized $FeCo_2$-NPC-900 obtained by pyrolysis at 900 °C exhibits more positive half-wave potential, higher diffusion-limited current density, and better stability than the state-of-the-art Pt/C, under both alkaline and acidic media. More importantly, the current synthetic approach based on MOFs offers a rational strategy to structure- and composition-controlled porous carbons for efficient electrocatalysis.

With increasing energy demand and environmental concerns, highly efficient electrochemical energy-storage and conversion devices, such as fuel cells and rechargeable metal–air batteries, have been considered as promising power sources. Although tremendous progress has been made, the sluggish kinetics of the oxygen reduction reaction (ORR) at the cathode limits the development of these devices.[1] Presently, platinum and its derivatives are the most efficient catalysts for ORR. However, the commercialization of Pt suffers from high cost, limited availability, poor stability, and susceptibility to methanol crossover.[2] In this regard, great effort has been made to explore Pt substitutes, among which heteroatom-doped (e.g., B, N, P, and S) porous carbons are the most promising.[3] The ORR performance of porous carbons strongly relies on the precursor type, dopant components, carbon support morphology, pore structure, and electronic conductivity, etc.[3–5] In contrast to the ORR activity over base metal oxides and/or metal-free carbon materials in basic solution only, M-N-doped porous carbons (M-NPC materials, M = Fe, Co) involving $FeN_x$ or $CoN_x$ species possess considerable ORR performance in both alkaline and acidic solutions, making it one of the most promising and universal systems for ORR.[4,5] Interestingly, although there have been only two reports on Fe,Co-codoped NPC (denoted as FeCo-NPC) electrocatalysts recently, they unambiguously present superior ORR performance compared to their Fe-NPC and Co-NPC counterparts, benefiting from the synergetic effect between highly active $FeN_x$ species and the enhanced corrosion resistance endowed by cobalt species.[5a,b]

Currently, most of M-NPC catalysts have been prepared by pyrolysis of the mixture of metal salt and nitrogen precursors including polypyrrole (PPy), polyaniline (PANI), cyanamide (CA), etc.[5c,6] Nevertheless, the unpredictable existence form of metal ions and nitrogen, inevitable agglomeration, and uncontrollable microstructure during pyrolysis remain as bottlenecks and might hamper the performance of these catalysts. Metalloporphyrin and its analogues, a definite structure with isolated metal ions locked by nitrogen, are ideal precursors to give Fe/Co-NPC catalysts with highly dispersed active sites.[5a,7] However, the metalloporphyrin molecules are prone to agglomerate randomly, making it hard to realize the high dispersion and accessibility of active sites in resultant pyrolysis products. Most recently, Feng and co-workers fabricated porous metalloporphyrinic polymers to greatly improve the porosity and ORR activity of resultant carbon involving alternative $FeN_x$ and $CoN_x$ species. Unfortunately, the metalloporphyrin motifs are hardly organized in an ordered way in porous polymers owing to their amorphous nature and the difficulty to precisely control the dispersion of Fe/Co-$N_x$ active sites.[5a] In view of this, it is highly desired to develop crystalline metalloporphyrinic frameworks as precursors to afford highly porous carbon doping with homogeneous $FeN_x$ and $CoN_x$ active species.

In this context, metal-organic frameworks (MOFs), a family of crystalline porous materials constructed by the coordination of metal ions and versatile organic linkers, should be ideal candidates.[8] The pyrolysis of MOFs is able to provide porous carbons with high surface area and homogeneous heteroatom dopants.[9] Most of these reports are based on zeolitic type of MOFs (ZIFs) as they provide high N contents and/or $CoN_x$ active sites in the products.[9a–i] To our knowledge, there has been only one report on the pyrolysis of porphyrinic MOF, which involves single metal ions in the porphyrin center, to afford porous carbon for ORR application.[10] Actually, the porphyrin centers can be occupied by different metal ions in a single MOF to give a multivariate MOF, in which different

[a] X. Fang,[+] L. Jiao,[+] Prof. Dr. S.-H. Yu, Prof. Dr. H.-L. Jiang
Hefei National Laboratory for Physical Sciences at the Microscale, CAS Key Laboratory of Soft Matter Chemistry, Collaborative Innovation Center of Suzhou Nano Science and Technology, Department of Chemistry
University of Science and Technology of China
Hefei, Anhui 230026 (P. R. China)
E-mail: jianglab@ustc.edu.cn
Homepage: http://staff.ustc.edu.cn/~jianglab/

[+] These authors contributed equally to this work.

Supporting Information and the ORCID identification number(s) for the author(s) of this article can be found under https://doi.org/10.1002/cssc.201700864.

metalloporphyrin motifs are well organized and dispersed. Upon pyrolysis, $MN_x$ species with different metals, possessing particular activity and functions, would be stabilized inside the carbon matrix to guarantee their high dispersion and display synergetic effect in catalysis. The high porosity of the resultant carbon, inherited from MOFs, would enable the active sites accessible to the electrolyte and substrate, thus leading to efficient ORR catalysis.

Considering this, a representative porphyrinic MOF, PCN-224,[11] with high stability and mesopores based on six-connected $Zr_6$ cluster and tetrakis(4-carboxyphenyl)porphyrin ($H_2$TCPP) ligand, was synthesized, followed by the porphyrin metalation with $Fe^{II}$ and $Co^{II}$ in different ratios to give PCN-224-$FeCo_x$ ($x$ is the feeding ratio of Co/Fe) in cubic shape. Upon pyrolysis and acid etching, PCN-224-$FeCo_x$ was converted to N-doped porous carbon nanocubes in a hollow structure involving highly dispersed $FeN_x$ and $CoN_x$ species, denoted as $FeCo_x$-NPC-$T$ ($T$ represents pyrolysis temperature) (Scheme 1).

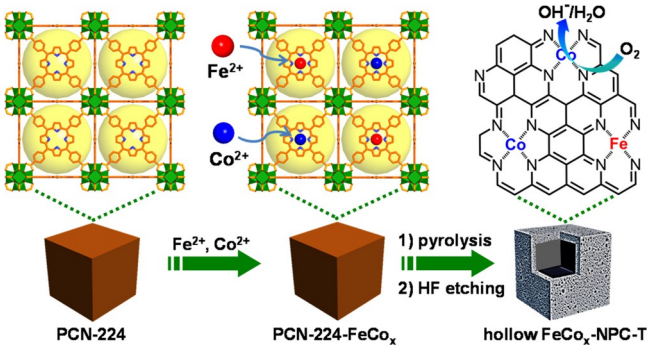


**Scheme 1.** Illustration of the stepwise fabrication of hollow porous $FeCo_x$-NPC-$T$ nanocubes with varying Co/Fe molar ratios at different pyrolysis temperatures.

The hollow porous structure of $FeCo_x$-NPC-$T$ guarantees the accessibility of active sites and efficient mass transfer. The coexistence of $FeN_x$ and $CoN_x$ species effectively integrates highly active catalytic centers and high graphitization of the carbon network. All characteristics above synergistically boost the ORR activity, and as a result, the optimized $FeCo_2$-NPC-900 composite exhibits superior electrocatalytic ORR performance compared to the state-of-the-art Pt/C in both alkaline and acidic solutions, including catalytic activity, long-term stability, and methanol tolerance capability.

The PCN-224 was chosen as it holds a 3D porous structure, very high surface area, and most importantly, the empty porphyrin centers ready to be metalated.[11] By postsynthetic metalation, the optimized PCN-224-$FeCo_2$ (a representative sample), in cubic shape with an average size of about 800 nm and a high BET surface area of 2100 $m^2 g^{-1}$ was obtained (Figures 1a and S1–S3), which was then transformed to $FeCo_2$-NPC-$T$ ($T$ = 800, 900, 1000) at different temperatures determined by thermogravimetric analysis in $N_2$ atmosphere, followed by HF etching (Figure S4). Taking the resultant $FeCo_2$-NPC-900 as an example, it inherited the cubic morphology and similar size from the parent PCN-224-$FeCo_2$ and exhibits a high BET surface area (1240 $m^2 g^{-1}$) with approximately 3 nm mesopores (Figures 1b and S5). TEM observation gives the sharp contrast between the inner cavity and outer carbon shell, indicating the hollow structure of $FeCo_2$-NPC-900, which can be also proved by the SEM image of the cracked hollow carbons (Figures 1c and S6). The formation of the hollow structure might be owed to the well-known Kirkendall-like effect.[12] Specifically, in the pyrolysis process, the Co and Fe species in PCN-224-$FeCo_2$ tend to flow outward at a high rate because of their large diffusion coefficients and then the pyrolysis product from organic ligands are graphitized around the outer Co/Fe species. When the carbon shell surpasses the critical thickness that can make it stable, then the structure collapse can be well inhibited, giving rise to the hollow structure of porous carbon. The thickness of the carbon shell is about 100 nm and no particles related to $ZrO_2$, Co, or Fe can be observed, aligning well with the powder X-ray diffraction (PXRD) results, which verify their complete removal by HF etching (Figures 1c and S7). Owing to the catalytic graphitization by Fe/Co species during pyrolysis, the HRTEM image clearly presents the lattice fringes with an interplanar space of 0.34 nm corresponding to the (002) plane of carbon (Figure 1d), which is in consistent with the peak at 26.0° in PXRD patterns (Figure S7). The graphitization degree of $FeCo_2$-NPC-900 can be further characterized by Raman scattering spectra. The D and G bands at 1332 and 1584 $cm^{-1}$ correspond to the disordered and $sp^2$-hybridized graphitic carbons, respectively, and the pretty low intensity ratio (1.02) of $I_D/I_G$ manifests the higher graphitization degree of $FeCo_2$-NPC-900 than Fe-NPC-900, corresponding to the sharp peaks in PXRD results and demonstrating the better effect of Co on graphitization than Fe (Figures S7 and S8). Elemental mapping suggests the coexistence of Fe, Co, N, and C elements and that Fe, Co, and N homogenously distribute throughout the carbon shell matrix and this further confirms the hollow structure of $FeCo_2$-NPC-900 (Figure 1e).

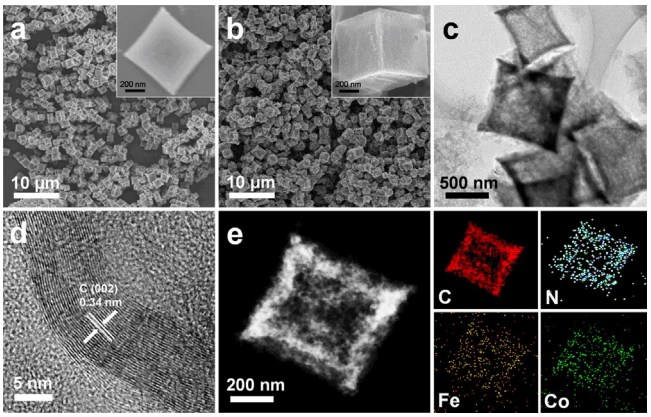


**Figure 1.** SEM images of (a) PCN-224-$FeCo_2$ and (b) $FeCo_2$-NPC-900 (inset in (a) and (b): enlarged single particle). (c) TEM, (d) high-resolution TEM (HRTEM), and (e) high-angle annular dark-field scanning TEM (HAADF-STEM) images and corresponding C, N, Fe, and Co elemental mappings for $FeCo_2$-NPC-900.

To further probe the chemical composition and M–N interaction in $FeCo_2$-NPC-900, X-ray photoelectron spectroscopy (XPS) was used. As shown in Figure 2a, the XPS survey spectrum clearly portrays the existence of C, N, O, Fe, and Co. The high-

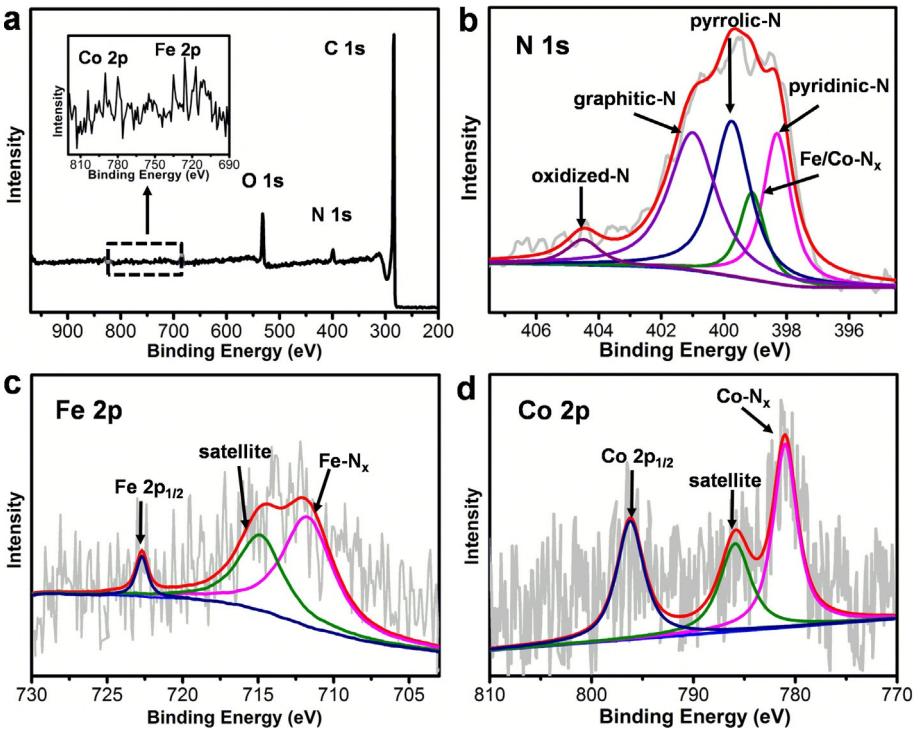


**Figure 2.** (a) XPS survey spectrum of $FeCo_2$-NPC-900. High-resolution XPS spectra of (b) N 1s, (c) Fe 2p, and (d) Co 2p of $FeCo_2$-NPC-900.

resolution N 1s spectrum fitted into five subpeaks reveals the presence of five types of N species: pyridinic N, graphitic N, pyrrolic N, M–$N_x$, and oxidized N (Figure 2b). To further confirm the chemical interaction between metal and nitrogen, the high-resolution XPS spectra of Fe 2p and Co 2p were investigated. They exhibit broad and weak peaks, possibly owing to the very low Fe/Co contents. The broad peaks centered at 710.8 and 780.6 eV are, respectively, assignable to Fe $3p_{3/2}$ and Co $3p_{3/2}$ (Figure 2c, d).[5a, 7b] The peak at 713.4 eV in the Fe 2p spectrum originated from chemical bonding between Fe and N confirms the existence of Fe–$N_x$ species.[4e, 5a] Similarly, the peak identified at 781.7 eV indicated the existence of Co–$N_x$, attributed to bonding between Co and N.[4c, 5b] To identify the real content of Fe and Co, inductively coupled plasma atomic emission spectrometry (ICP-AES) was performed. It can be seen that the actual Fe and Co contents in $FeCo_2$-NPC-900 are 0.43 and 0.37 wt%, respectively (Table S1).The XPS and ICP-AES results above highlight the presence of Fe/Co–N bond as potential ORR active sites in $FeCo_2$-NPC-900.

Encouraged by the results above, the ORR activity of the $FeCo_x$-NPC-900 was first evaluated in alkaline solution using rotating disk electrode (RDE). The cyclic voltammetry (CV) curves for all samples exhibit a well-defined cathodic peak at 0.8–1.0 V in $O_2$-saturated 0.1 M KOH, revealing their electrocatalytic activities (Figure 3a). The presence of the highest reduction peak centered at 0.9 V for $FeCo_2$-NPC-900 predicts its superior ORR activity among all $FeCo_x$-NPC-900 samples. Linear sweep voltammetry (LSV) curves performed on a RDE at a scan rate of 5 mV $s^{-1}$ show that $FeCo_2$-NPC-900 possesses prominent catalytic activity with values of onset potential of 0.97 V, half-wave potential of 0.87 V, and diffusion-limited current density of −5.5 mA $cm^{-2}$, which are better than those of Pt/C and most of the reported non-noble metal catalysts (Figure 3b, Table S2). Additionally, the LSV curve of Pt/C was tested three times to confirm the reliability of the data (Figure S9). In contrast, the monometallic Fe-NPC-900 and Co-NPC-900 present inferior activity, suggesting synergetic promotion effect between $FeN_x$ and $CoN_x$ active sites in $FeCo_2$-NPC-900 (Figure 3b). Moreover, the kinetic current density of $FeCo_2$-NPC-900 was calculated to be 7.80 mA $cm^{-2}$ at 0.85 V, which is also higher than that of Pt/C, whereas the Fe-NPC-900 and Co-NPC-900 exhibit lower kinetic current density, which further confirms the synergetic effect (Table S3). Furthermore, the $FeCo_2$-NC-900-mix sample obtained from the physical mixture of TCPP-Fe and TCPP-Co was also tested and exhibited inferior activity for ORR (Figure S10), confirming the superiority of $FeCo_2$-NPC-900 derived from PCN-224-$FeCo_2$. Control experiments for samples with various Fe/Co ratios at different pyrolysis temperatures demonstrate that the 1:2 Fe/Co feeding molar ratio and 900 °C conditions are optimal parameters for achieving the best ORR activity (Figures S9 and S10). Therefore, $FeCo_2$-NPC-900 will be investigated in detail as a representative sample hereafter.

To assess the ORR electron-transfer mechanism for $FeCo_2$-NPC-900, RDE measurements were conducted at various rotation rates from 400 to 2400 rpm, showing well-defined curves of diffusion-limited current density and increasing current densities with increasing rotation speed (Figure 3c). The electron-transfer number was calculated to be 3.9 according to the Koutecky–Levich (K–L) equation, illustrating the ideal 4 $e^-$ oxygen reduction process (Figure 3c, inset). The Tafel slope was calculated to be −78 mV $dec^{-1}$, much lower than −86 mV $dec^{-1}$ for Pt/C, signifying its more favorable kinetic behavior (Figure S13). The Nyquist plots indicate that $FeCo_2$-NPC-900 possesses comparable charge-transfer resistance to Co-

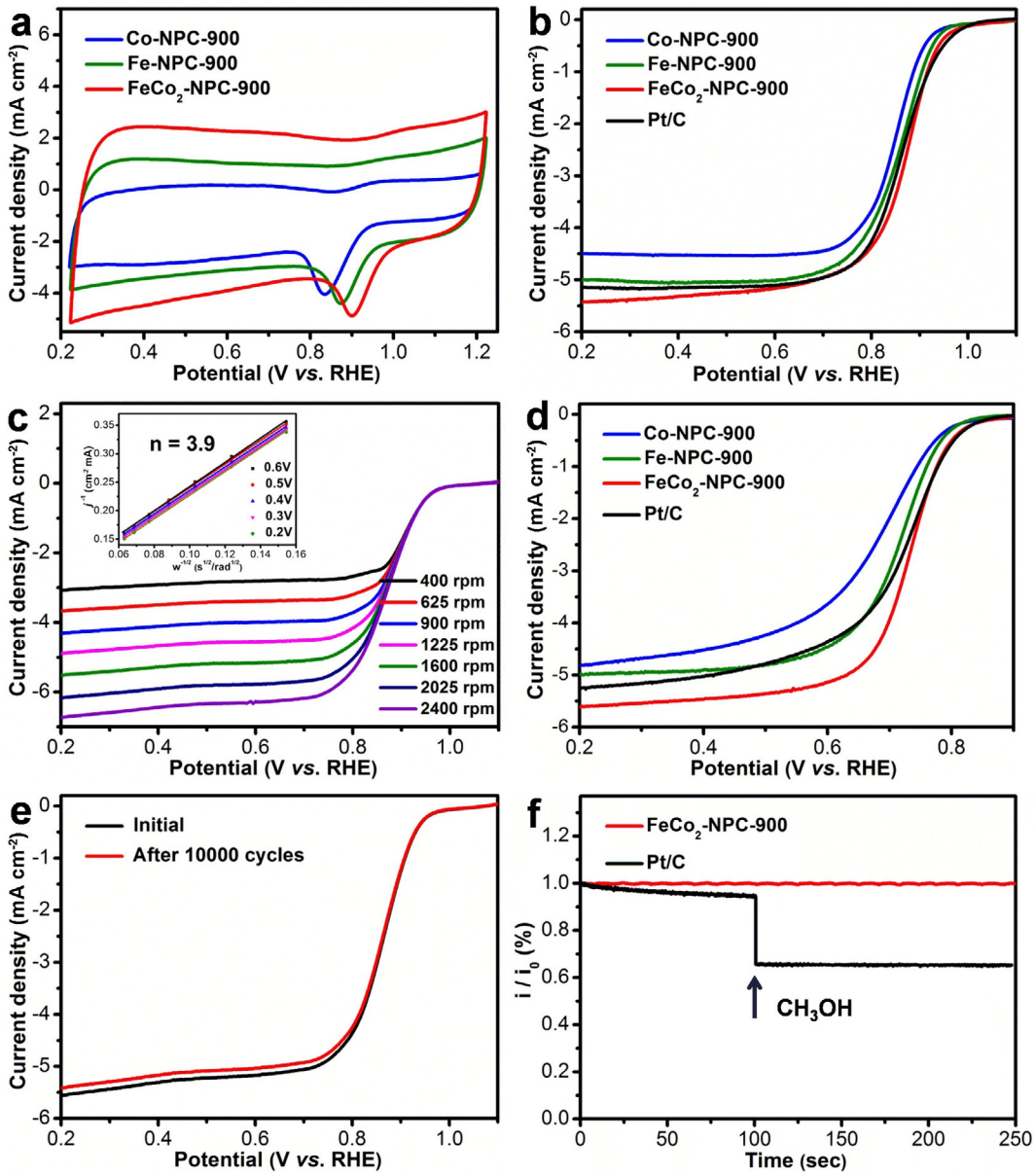


**Figure 3.** (a) CV curves and (b) LSV curves for different samples in $O_2$-saturated 0.1 M KOH solution; (c) LSV curves at different RDE rotation rates for $FeCo_2$-NPC-900 in $O_2$-saturated 0.1 M KOH solution (inset: K–L plots and electron transfer numbers at different potentials); (d) LSV curves for different samples in $O_2$-saturated 0.1 M $HClO_4$ solution; (e) LSV curves of $FeCo_2$-NPC-900 before and after 10000 cycles in $O_2$-saturated 0.1 M KOH solution and (f) methanol-tolerance evaluation for $FeCo_2$-NPC-900 and the Pt/C in 0.1 M KOH solution.

NPC-900, but significantly smaller than Fe-NPC-900 (Figure S14), reflecting that the Co species mainly contributes to its high graphitization and conductivity, which is highly consistent with PXRD and Raman spectra results indicated above (Figures S7 and S8).

Although it is more challenging to obtain an efficient ORR catalyst in acidic solution, thanks to the $FeN_x$ and $CoN_x$ species involved, $FeCo_2$-NPC-900 also exhibits excellent ORR performance, surpassing its counterparts, in 0.1 M $HClO_4$ solution. The CV curve indicates a significant reduction process with a pronounced cathodic ORR peak at approximately 0.6 V in $O_2$-saturated 0.1 M $HClO_4$ (Figure S15). Remarkably, it shows more positive half-wave potential (0.74 V) and much higher diffusion-limiting current ($-0.56$ mA cm$^{-2}$), than Pt/C and the corresponding Fe (or Co)-NPC-T (Figures 3d, S16, and S17), as well as most of non-noble metal catalysts previously reported (Table S4). To confirm the ORR performance of Pt/C, the LSV curves tested three times show the high reliability of the data (Figure S18). The K–L plots from RDE polarization curves between 0.2 to 0.6 V exhibit good parallel straight lines, and the transferred electron number per $O_2$ molecule was calculated to be 3.9, suggesting a 4 e$^-$ ORR pathway even in acidic solution (Figure S19). The lower Tafel slope of $FeCo_2$-NPC-900 ($-71$ mV dec$^{-1}$) and larger kinetic current density (11.48 mA cm$^{-2}$) than Pt/C further reflect its more favorable kinetic behavior (Figure S20, Table S3). Notably, although much effort has been made, there are very limited catalysts outperforming Pt/C for ORR in both alkaline and acidic solutions

(Table S5), which further highlights the great advantages of $FeCo_2$-NPC-900 in ORR catalysis. To further correlate the ORR activity with the formation of $FeN_x$ and $CoN_x$, $SCN^-$ ion (with a high affinity to $M–N_x$ sites) was used to poison $M–N_x$ sites. As shown in Figure S21, the $E_{onset}$ and $E_{1/2}$ of $FeCo_2$-NPC-900 negatively shift by 45 and 84 mV, respectively, after the addition $SCN^-$. These experimental studies clearly elucidate that $FeN_x$ and $CoN_x$ sites are the origin of the ORR activity of $FeCo_2$-NPC-900.

In addition to the high activity, excellent stability and methanol tolerance are also necessary for an ideal ORR catalyst. The polarization curve recorded after 10000 cycles of continuous CV scanning for $FeCo_2$-NPC-900 shows negligible difference from the initial one in both 0.1 M KOH and 0.1 M $HClO_4$ (Figures 3e and S22), exemplifying its outstanding stability, in reference to the activity decline (an approximate 65 and 43 mV negative shift of the half-wave potential in alkaline and acid solutions, respectively) of the commercial Pt/C catalyst (Figure S23). Chronoamperometry tests were also conducted and demonstrate good activity during 20000 s of continuous operation (Figure S24), further showing great stability. Moreover, almost no variation in the current can be observed upon methanol addition for $FeCo_2$-NPC-900 in both solutions, in stark contrast to the abrupt change for the Pt/C catalyst (Figures 3f and S25). The results demonstrate that $FeCo_2$-NPC-900 has strong tolerance against the crossover effect, making it a promising catalyst for direct methanol fuel cells. The excellent stability can be attributed to the highly graphitized nanostructures, and strong bonding between Fe/Co and N, as well as highly dispersed Fe/Co-$N_x$ active sites.[5a]

In summary, starting with a porphyrinic metal–organic framework (MOF), PCN-224-$FeCo_x$, involving tunable molar ratio of $Fe^{II}$ and $Co^{II}$ alternatively residing inside the porphyrin centers, as a single precursor (i.e., in the absence of additional metal species or nitrogen/carbon sources), hollow porous carbon nanocubes enriched with uniformly dispersed $FeN_x$ and $CoN_x$ active sites were successfully prepared in a controlled manner. The crystalline porous structure of PCN-224-$FeCo_x$ effectively prevents the agglomeration of metalloporphyrin motifs and allows homogeneous dispersion of active sites. As far as we know, this is the first work on the simultaneous generation of $FeN_x$ and $CoN_x$ active species from crystalline precursors. Benefiting from the unique hollow porous nanostructure, along with the synergetic effect between the highly dispersed $FeN_x$ (offering superior activity) and $CoN_x$ (contributing to high graphitization) sites, the optimized $FeCo_2$-NPC-900 catalyst exhibits excellent oxygen reduction reaction (ORR) electrocatalytic activity, favorable reaction kinetics, long-term stability, and superior methanol tolerance under both alkaline and acidic conditions, surpassing the state-of-the-art Pt/C and most of the non-noble metal electrocatalysts. The facile, rational, and controllable strategy demonstrated herein opens up a new avenue for the fabrication of high-performance non-noble metal electrocatalysts, on the basis of crystalline MOFs with tunable and modifiable organic linkers.

## Experimental Section

### Preparation of catalysts

**Synthesis of organic ligand**: The tetrakis(4-carboxyphenyl)porphyrin ($H_2TCPP$) was synthesized based on previous reports with minor modifications.[11] Typically, pyrrole (3.0 g, 0.043 mol) and methyl *p*-formylbenzoate (6.9 g, 0.042 mol) were added into a 250 mL three-necked flask with propionic acid (100 mL). The solution was refluxed at 160 °C for 12 h and then cooled down to room temperature. The precipitate was obtained by filtration, washing with ethanol, ethyl acetate and tetrahydrofuran, and finally drying in vacuum overnight. Then the obtained precipitate (1.95 g) was dissolved with THF (60 mL) and MeOH (60 mL) in a three-necked flask, then a solution of KOH (6.82 g) dissolved in $H_2O$ (60 mL) was added. This mixture solution was refluxed at 80 °C for 12 h and subsequently cooled down to room temperature. Additional $H_2O$ was added to make sure the solid was completely dissolved and then the solution was acidified with 1 M HCl until no more purple precipitate generated. The purple solid was filtrated, washed with water, and dried in vacuum.

**Synthesis of PCN-224**: PCN-224 was prepared based on the reported procedure with minor modifications.[11] Typically, $ZrCl_4$ (120 mg), $H_2TCPP$ (50 mg), and benzoic acid (1200 mg) in DMF (8 mL) were ultrasonically dissolved in a 20 mL Pyrex vial. The mixture was heated in 120 °C oven for 24 h. After cooling down to room temperature, cubic dark purple crystals were harvested by filtration.

**Synthesis of PCN-224-$FeCo_x$**: Typically, PCN-224 (200 mg) with a desired molar ratio of $FeCl_2{\cdot}4H_2O$ and $CoCl_2{\cdot}6H_2O$ (1.50 mmol $FeCl_2{\cdot}4H_2O$ and 0.75 mmol $CoCl_2{\cdot}6H_2O$ for PCN-224-$FeCo_{0.5}$; 1.125 mmol $FeCl_2{\cdot}4H_2O$ and 1.125 mmol $CoCl_2{\cdot}6H_2O$ for PCN-224-$FeCo_1$; 0.75 mmol $FeCl_2{\cdot}4H_2O$ and 1.50 mmol $CoCl_2{\cdot}6H_2O$ for PCN-224-$FeCo_2$) in DMF were heated at 120 °C with stirring for 12 h. After that, the mixture was centrifuged. The liquid was decanted and the remaining solid was washed twice with fresh DMF and twice with acetone. The acetone was decanted, and the sample was dried in an oven. PCN-224-Fe and PCN-224-Co were synthesized through a similar procedure by using only $FeCl_2{\cdot}4H_2O$ (2.25 mmol) or $CoCl_2{\cdot}6H_2O$ (2.25 mmol), respectively.

**Synthesis of $FeCo_x$-NPC-900**: Typically, PCN-224-$FeCo_x$ powder (100 mg) was heated to 900 °C with a heating rate of 5 °C $min^{-1}$ and pyrolyzed at 900 °C for 2 h under flowing $N_2$ atmosphere, and then cooled to room temperature naturally to obtain porous carbon composite materials. Then, the involved metal or metal oxide nanoparticles in the resultant products were etched twice with HF solution at 80 °C for 12 h, and washed thoroughly with lots of water to yield $FeCo_x$-NPC-900 catalysts. Finally, the products were dried in vacuum at 120 °C overnight prior to use.

**Synthesis of $FeCo_2$-NC-900-mix**: The $FeCo_2$-NC-900-mix was obtained through the similar procedure with $FeCo_2$-NPC-900 started from the physical mixture of TCPP-Fe and TCPP-Co.

### Electrochemical performance evaluation

**Synthesis and electrochemical measurements of working electrode**: Electrochemical measurements were performed with a CHI 760E electrochemical analyzer (CH Instruments, Inc., Shanghai) and

a rotating disk electrode (RDE) (Pine Instruments, Grove city, PA). All electrochemical measurements were conducted in a typical three-electrode setup with a Pt counter electrode and Ag/AgCl reference electrodes and with 0.1 M KOH or $HClO_4$ as the electrolyte. The electrolyte was saturated with oxygen by bubbling $O_2$ prior to each experiment. A flow of $O_2$ was maintained over the electrolyte during the measurements in order to ensure $O_2$ saturation. The catalyst ink was prepared by dispersing the catalyst (2 mg) into ethanol solvent (1 mL) containing 5 wt% Nafion (10 μL) and sonicated for 30 min. Then, the catalyst ink (30 μL) was loaded onto a glassy carbon electrode (GCE) of 5 mm diameter (loading amount $\approx$0.30 mg cm$^{-2}$). The LSV measurements of the catalysts were determined using a RDE (Pine Instruments, Grove city, PA). The scan rate of the working electrode was 5 mV s$^{-1}$ with varying rotating speed from 400 to 2400 rpm. The number of electrons transferred ($n$) during ORR was calculated by Koutecky–Levich equation, at various electrode potentials:

$$\frac{1}{j}=\frac{1}{j_L}+\frac{1}{J_K}=\frac{1}{B\omega^{1/2}}+\frac{1}{j_K} \quad (1)$$

$$B=0.62\,n\,F\,C_0\,(D_0)^{2/3}\,\nu^{-1/6} \quad (2)$$

where $j$ is the measured current density; $j_k$ and $j_L$ are the kinetic and diffusion-limiting current densities, respectively; $\omega$ is the angular velocity of the disk ($\omega=2\pi N$, $N$ is the linear rotation speed); $n$ represents the overall number of electrons transferred in oxygen reduction; $F$ is the Faraday constant ($F=96\,485$ C mol$^{-1}$); $C_0$ is the bulk concentration of $O_2$ ($1.2\times10^{-6}$ mol cm$^{-3}$); $D_0$ is the diffusion coefficient of $O_2$ in 0.1 M KOH and 0.1 M $HClO_4$ ($1.9\times10^{-5}$ cm$^2$ s$^{-1}$), and $\nu$ is the kinematic viscosity of the electrolyte (0.01 cm$^2$ s$^{-1}$).

## Acknowledgements

*This work is supported by the NSFC (21371162, 21673213 and 21521001), the National Research Fund for Fundamental Key Project (2014CB931803), the Recruitment Program of Global Youth Experts and Key Laboratory of Functional Inorganic Material Chemistry (Heilongjiang University), Ministry of Education.*

## *Conflict of interest*

*The authors declare no conflict of interest.*

**Keywords:** doping · electrocatalysis · metal–organic frameworks · oxygen reduction reaction · porous carbon

[1] a) R. Bashyam, P. Zelenay, *Nature* **2006**, *443*, 63; b) Z. Chen, D. Higgins, A. Yu, L. Zhang, J. Zhang, *Energy Environ. Sci.* **2011**, *4*, 3167; c) W. He, Y. Wang, C. Jiang, L. Lu, *Chem. Soc. Rev.* **2016**, *45*, 2396; d) M. Shao, Q. Chang, J.-P. Dodelet, R. Chenitz, *Chem. Rev.* **2016**, *116*, 3594; e) W. Xia, A. Mahmood, Z. Liang, R. Zou, S. Guo, *Angew. Chem. Int. Ed.* **2016**, *55*, 2650; *Angew. Chem.* **2016**, *128*, 2698.

[2] a) J. Wu, J. Zhang, Z. Peng, S. Yang, F. T. Wagner, H. Yang, *J. Am. Chem. Soc.* **2010**, *132*, 4984; b) X. Han, F. Cheng, T. Zhang, J. Yang, Y. Hu, J. Chen, *Adv. Mater.* **2014**, *26*, 2047.

[3] a) J. Zhang, L. Dai, *ACS Catal.* **2015**, *5*, 7244; b) Y. Zhao, L. Yang, S. Chen, X. Wang, Y. Ma, Q. Wu, Y. Jiang, W. Qian, Z. Hu, *J. Am. Chem. Soc.* **2013**, *135*, 1201; c) G. Wang, Y. Sun, D. Li, H.-W. Liang, R. Dong, X. Feng, K. Müllen, *Angew. Chem. Int. Ed.* **2015**, *54*, 15191; *Angew. Chem.* **2015**, *127*, 15406; d) D.-S. Yang, D. Bhattacharjya, S. Inamdar, J. Park, J.-S. Yu, *J. Am. Chem. Soc.* **2012**, *134*, 16127; e) J. Duan, S. Chen, M. Jaroniec, S. Z. Qiao, *ACS Catal.* **2015**, *5*, 5207.

[4] a) J. Masa, W. Xia, M. Muhler, W. Schuhmann, *Angew. Chem. Int. Ed.* **2015**, *54*, 10102; *Angew. Chem.* **2015**, *127*, 10240; b) Z.-Y. Wu, X.-X. Xu, B.-C. Hu, H.-W. Liang, Y. Lin, L.-F. Chen, S.-H. Yu, *Angew. Chem. Int. Ed.* **2015**, *54*, 8179; *Angew. Chem.* **2015**, *127*, 8297; c) Y.-Z. Chen, C. Wang, Z.-Y. Wu, Y. Xiong, Q. Xu, S.-H. Yu, H.-L. Jiang, *Adv. Mater.* **2015**, *27*, 5010; d) Y. Hou, Z. Wen, S. Cui, S. Ci, S. Mao, J. Chen, *Adv. Funct. Mater.* **2015**, *25*, 872; e) W.-J. Jiang, L. Gu, L. Li, Y. Zhang, X. Zhang, L.-J. Zhang, J.-Q. Wang, J.-S. Hu, Z. Wei, L.-J. Wan, *J. Am. Chem. Soc.* **2016**, *138*, 3570.

[5] a) Q. Lin, X. Bu, A. Kong, C. Mao, F. Bu, P. Feng, *Adv. Mater.* **2015**, *27*, 3431; b) T. Palaniselvam, V. Kashyap, S. N. Bhange, J.-B. Baek, S. Kurungot, *Adv. Funct. Mater.* **2016**, *26*, 2150; c) G. Wu, K. L. More, C. M. Johnston, P. Zelenay, *Science* **2011**, *332*, 443; d) B. Xia, Y. Yan, N. Li, H. Wu, X. W. Lou, X. Wang, *Nat. Energy* **2016**, *1*, 15006; e) Z. Xiang, Y. Xue, D. Cao, L. Huang, J.-F. Chen, L. Dai, *Angew. Chem. Int. Ed.* **2014**, *53*, 2433; *Angew. Chem.* **2014**, *126*, 2465.

[6] a) J. Zhang, Z. Zhao, Z. Xia, L. Dai, *Nat. Nanotechnol.* **2015**, *10*, 444; b) X.-H. Li, S. Kurasch, U. Kaiser, M. Antonietti, *Angew. Chem. Int. Ed.* **2012**, *51*, 9689; *Angew. Chem.* **2012**, *124*, 9827; c) J. Tang, J. Liu, C. Li, Y. Li, M. O. Tade, S. Dai, Y. Yamauchi, *Angew. Chem. Int. Ed.* **2015**, *54*, 588; *Angew. Chem.* **2015**, *127*, 598; d) H.-W. Liang, X. Zhuang, S. Brüller, X. Feng, K. Müllen, *Nat. Commun.* **2014**, *5*, 4973.

[7] a) C. W. B. Bezerra, L. Zhang, K. Lee, H. Liu, A. L. B. Marques, E. P. Marques, H. Wang, J. Zhang, *Electrochim. Acta* **2008**, *53*, 4937; b) M. Jahan, Q. Bao, K. P. Loh, *J. Am. Chem. Soc.* **2012**, *134*, 6707; c) H. Tang, H. Yin, J. Wang, N. Yang, D. Wang, Z. Tang, *Angew. Chem. Int. Ed.* **2013**, *52*, 5585; *Angew. Chem.* **2013**, *125*, 5695.

[8] a) H.-C. Zhou, J. R. Long, O. M. Yaghi, *Chem. Rev.* **2012**, *112*, 673; b) H.-C. Zhou, S. Kitagawa, *Chem. Soc. Rev.* **2014**, *43*, 5415; c) B. Li, H.-M. Wen, Y. Cui, W. Zhou, G. Qian, B. Chen, *Adv. Mater.* **2016**, *28*, 8819; d) Q.-L. Zhu, Q. Xu, *Chem. Soc. Rev.* **2014**, *43*, 5468; e) L. Jiao, Y.-X. Zhou, H.-L. Jiang, *Chem. Sci.* **2016**, *7*, 1690; f) G. Cai, W. Zhang, L. Jiao, S.-H. Yu, H.-L. Jiang, *Chem* **2017**, *2*, 791; g) Q. Yang, Q. Xu, H.-L. Jiang, *Chem. Soc. Rev.* **2017**, DOI: https://doi.org/10.1039/c6cs00724d.

[9] a) S. Ma, G. A. Goenaga, A. V. Call, D.-J. Liu, *Chem. Eur. J.* **2011**, *17*, 2063; b) H.-L. Jiang, B. Liu, Y.-Q. Lan, K. Kuratani, T. Akita, H. Shioyama, F. Zong, Q. Xu, *J. Am. Chem. Soc.* **2011**, *133*, 11854; c) D. Zhao, J.-L. Shui, C. Chen, X. Chen, B. M. Reprogle, D. Wang, D.-J. Liu, *Chem. Sci.* **2012**, *3*, 3200; d) P. Zhang, F. Sun, Z. Xiang, Z. Shen, J. Yun, D. Cao, *Energy Environ. Sci.* **2014**, *7*, 442; e) W. Zhang, Z.-Y. Wu, H.-L. Jiang, S.-H. Yu, *J. Am. Chem. Soc.* **2014**, *136*, 14385; f) H. Zhong, J. Wang, Y. Zhang, W. Xu, W. Xing, D. Xu, Y. Zhang, X. Zhang, *Angew. Chem. Int. Ed.* **2014**, *53*, 14235; *Angew. Chem.* **2014**, *126*, 14459; g) B. You, N. Jiang, M. Sheng, W. S. Drisdell, J. Yano, Y. Sun, *ACS Catal.* **2015**, *5*, 7068; h) Z. Li, M. Shao, L. Zhou, R. Zhang, C. Zhang, M. Wei, D. G. Evans, X. Duan, *Adv. Mater.* **2016**, *28*, 2337; i) L. Shang, H. Yu, X. Huang, T. Bian, R. Shi, Y. Zhao, G. I. N. Waterhouse, L.-Z. Wu, C.-H. Tung, T. Zhang, *Adv. Mater.* **2016**, *28*, 1668; j) M. Hu, J. Reboul, S. Furukawa, N. L. Torad, Q. Ji, P. Srinivasu, K. Ariga, S. Kitagawa, Y. Yamauchi, *J. Am. Chem. Soc.* **2012**, *134*, 2864; k) S. Zhao, H. Yin, L. Du, L. He, K. Zhao, L. Chang, G. Yin, H. Zhao, S. Liu, Z. Tang, *ACS Nano* **2014**, *8*, 12660; l) Y.-T. Xu, X. Xiao, Z.-M. Ye, S. Zhao, R. Shen, C.-T. He, J.-P. Zhang, Y. Li, X.-M. Chen, *J. Am. Chem. Soc.* **2017**, *139*, 5285; m) H. Tabassum, W. Guo, W. Meng, A. Mahmood, R. Zhao, Q. Wang, R. Zou, *Adv. Energy Mater.* **2017**, *7*, 1601671.

[10] Q. Lin, X. Bu, A. Kong, C. Mao, X. Zhao, F. Bu, P. Feng, *J. Am. Chem. Soc.* **2015**, *137*, 2235.

[11] D. Feng, W.-C. Chung, Z. Wei, Z.-Y. Gu, H.-L. Jiang, Y.-P. Chen, D. J. Darensbourg, H.-C. Zhou, *J. Am. Chem. Soc.* **2013**, *135*, 17105.

[12] a) Y. Yin, R. M. Rioux, C. K. Erdonmez, S. Hughes, G. A. Somorjai, A. P. Alivisatos, *Science* **2004**, *304*, 711; b) W. Wang, M. Dahl, Y. Yin, *Chem. Mater.* **2013**, *25*, 1179; c) H. Hu, J. Zhang, B. Guan, X. W. Lou, *Angew. Chem. Int. Ed.* **2016**, *55*, 9514; *Angew. Chem.* **2016**, *128*, 9666.

Manuscript received: June 17, 2017

Accepted manuscript online: July 3, 2017
Version of record online: July 17, 2017